Results in Engineering 7 (2020) 100155

Contents lists available at ScienceDirect

Results in Engineering

journal homepage: www.editorialmanager.com/rineng/Default.aspx

Laser powder bed fusion of Ti15Mo

Thywill Cephas Dzogbewu

Department of Mechanical and Mechatronics Engineering, Central University of Technology, Free State, Bloemfontein, South Africa

ARTICLE INFO

Keywords:
LPBF
Ti15Mo
Alloy
Microstructure
Engineering
And biomedical applications

ABSTRACT

Ti15Mo is a generic alloy that has been around for a long time, however, it could not attain widespread applications compared to the Ti6Al4V due to the inherent limitations of the conventional methods of manufacturing the alloy. Laser powder bed fusion (LPBF) an additive manufacturing technology was used to determine the possibility of manufacturing the Ti15Mo alloy with improved mechanical properties for widespread applications. 85 wt% of Ti was mechanically mixed with 15 wt% Mo and in situ alloyed by the laser beam. The laser beam could not melt the Mo powder particles completely due to the thermophysical differences between the elemental powders. The ultimate tensile strength and the microhardness results obtained for the LPBF Ti15Mo samples were within the range of Ti15Mo alloy manufactured by conventional methods, which indicated that LPBF technology could be used to in situ alloy different elemental powders with mechanical properties comparable to samples manufactured using the conventional methods. The ductility of the LPBF Ti15Mo samples was lower than samples manufactured using conventional methods. The low ductility value was attributed to the high rate of heating and cooling simultaneously by the LPBF process.

1. Introduction

β-type Ti alloys have attracted great research interests, probably due to the wide range of mechanical properties they can provide for engineering and biomedical applications. A survey of the literature revealed that the binary Ti15Mo alloy has taken the center stage and has become the main focus of many researchers [1], probably due to its low elastic modulus, high strength, excellent fatigue strength, good ductility/formability, and exceptional corrosion resistance. The Ti15Mo is a generic alloy that has been around for a long time, however, unlike the Ti6Al4V alloy which is widely used in the aerospace and the biomedical industries, the Ti15Mo has never found wide applications in engineering but has attracted significant attention in the medical and surgical device industry for about three decades [2,3]. Two important factors held Ti15Mo back from widespread applications: "the physical metallurgy of the alloy and the inability of the then-current reactive metals melting and processing machinery to handle this unusual binary alloy" [3]. The inherent limitations of the conventional methods resulted in the production of the alloy with metallurgical defects, such as porosity, shrinkage, and inhomogeneous microstructure which adversely affect the mechanical properties of the alloy hence its limited applications [3,4]. Conventionally the Ti15Mo alloy products are machine from Ti15Mo bar stocks which are manufactured using the vacuum arc melting process. The production of the Ti15Mo bar stocks and the subsequent subtractive process of machining make the entire process of producing the Ti15Mo products conventionally very expensive and waste of material. Laser powder bed fusion (LPBF) which is a subset of additive manufacturing (AM) is currently considered as the renaissance of the manufacturing industry and would probably manufacture the Ti15Mo alloy without the above-mentioned metallurgical defects at a lower cost, as a result of the additive manufacturing process as opposed the subtractive manufacturing process [5–7].

Pre-alloyed powders are the desired feedstocks for the LPBF process. However, the production of the pre-alloyed powder required manufacturing billets, wires, sheets, etc. of the intended alloyed before converting it into spherical gas atomized pre-alloyed powder [8]. Before commercializing novel pre-alloy powder, it is logically required to develop confidence in the material's processability and properties. This would require further metallurgical analysis on batch elements [9,10]. These multiply steps involved in the production of the pre-alloyed powders make the whole production process of pre-alloyed powders capital intensive, especially when developing new pre-alloyed powders. Such developmental steps that are capital intensive can inhibit the experimental development of novel alloys. From basic economics, it is proven that if the initial input material for production is expensive the final product is likely to be very expensive [9]. To possibly reduce the cost of manufacturing the Ti15Mo alloy with improved mechanical integrity and to enhance the possibility of its widespread application; the

E-mail address: thydzo@yahoo.fr.

https://doi.org/10.1016/j.rineng.2020.100155
Received 9 April 2020; Received in revised form 15 June 2020; Accepted 8 July 2020

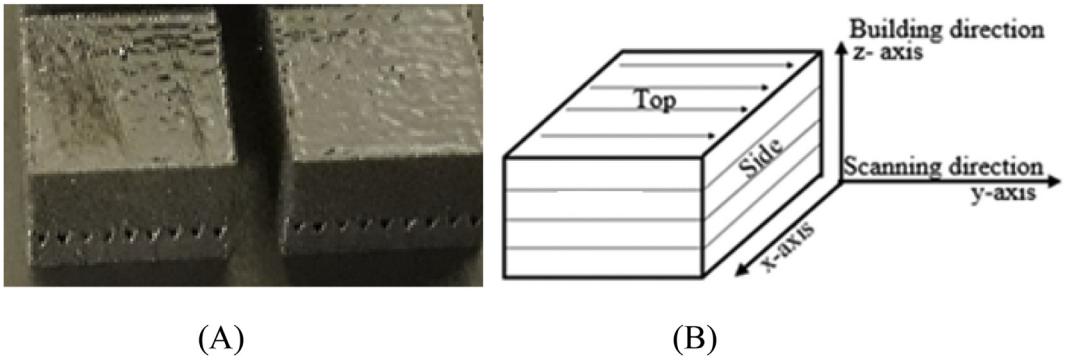

Fig. 1. LPBF Ti15Mo samples (A) The laser scanning coordination system (the top will be referred to as perpendicular direction and the side longitudinal direction (B).

LPBF process would be used to in-situ alloy Ti and Mo elemental powders. In-situ alloying using the LPBF would enable a faster, more cost-effective development of new pre-alloyed powders which could be used for both conventional and additive manufacturing processes. Easy processing (cost-effective) of different elemental powders would certainly broaden the material database for additive manufacturing [10,11]. Successful realization of using the AM process for in-situ alloying and not relying on pre-alloyed powders would give the material scientist great freedom of mixing different elemental powders for specific engineering and biomedical applications [12,13]. The possibility of tailoring alloying content to induce a particular microstructure and meeting a specific required mechanical property makes in-situ alloying via LPBF a prime technology of the day.

The LPBF process of manufacturing is an evolutional paradigm shift from the conventional methods of fabrications. The conventional methods (Turning, milling, grinding, drilling, etc.) of manufacturing involved part-specific tooling (subtractive manufacturing) as opposed to the additive manufacturing strategy used by the LPBF technology. The high degree of freedom offered by the LPBF technology of building complex geometries that would otherwise be difficult or impossible to produce using conventional manufacturing processes makes it a preferable choice for high-value markets [14,15]. The one-step manufacturing potency of the AM process eliminated the need for assembling multiple components [8], which would greatly reduce the cost of manufacturing [10]. The LPBF manufacturing process would permit the manufacturing of near-net-shapes with the possibility of production intricate biomimetic structures and engineering products with customized geometries.

2. Materials and methods

The samples were manufactured with spherical argon atomized Ti (CpTi, grade 2) and Mo powders procured from TLS Technik. The powder characteristics were specified by the supplier. The chemical composition of the Ti powder is presented in wt.%: Ti (bal.), O (0.17), Fe (0.062), C (0.006), H (0.002), N (0.012). The 10th, 50th and 90th percentiles of equivalent diameter (weighted by volume) of the powder Ti particles were d10 = 11.6 μm, d50 = 24.6 μm and d90 = 38.4 μm. The percentiles equivalent diameter of the Mo powder was d10 = 10.9 μm, d50 = 22.4 μm and d90 = 31.9 μm 15 wt% of Mo was mechanically mixed with 85 wt % of the CpTi powder until a homogenous mixture was obtained. The mixture of Ti15%Mo was dried in an oven for about 15 h at a temperature of 85 °C. The powder was stirred at 30 min interval.

EOSINT M280 machine (EOS GmbH) equipped with 400 W Yb-fibre laser was used for manufacturing the Ti15Mo alloy by in situ alloying the elemental powders. The Ti15Mo samples were manufactured with optimum process parameters at a laser power of 150 W with a corresponding scanning speed of 1.0 m/s and a hatch distance of 80 μm based on the initial results presented elsewhere [16] according to the algorithm proposed by Yadroitsev et al. [17]. The laser spot size diameter was 80 μm and CpTi plate was used as the substrate. The powder layer thickness was 30 μm. The samples were of a dimension of 10 mm × 10 mm x 10 mm (length x width x thickness). The samples were stress relieved in an argon atmosphere at a temperature of 650 °C for 3 h and were cut from the base plate using electrical discharge machining and cross-section into smaller units for mounting.

The samples were metallurgically prepared for optical and scanning

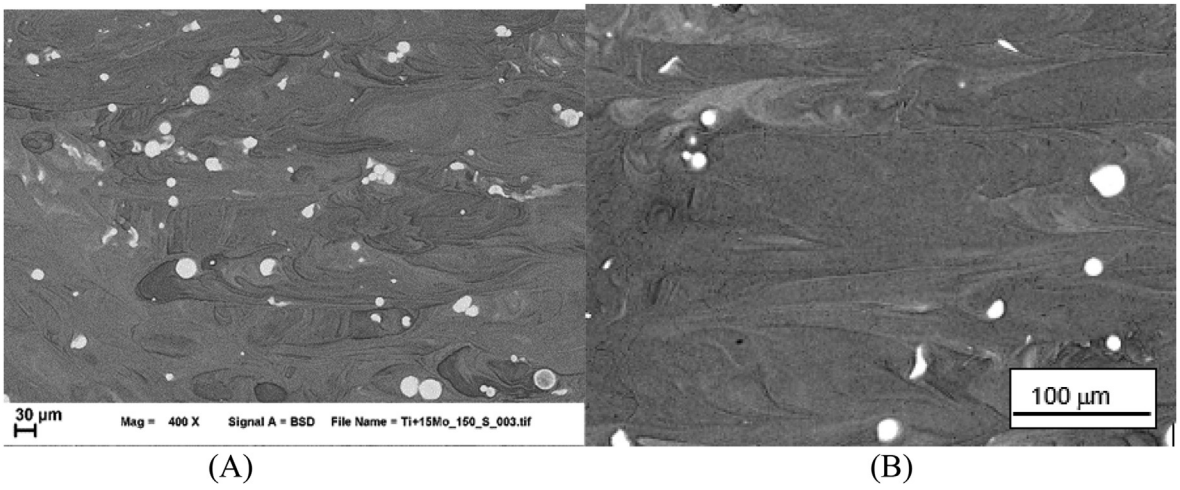

Fig. 2. SEM image of the TI15Mo in BSE mode (A) Perpendicular view (B) Longitudinal view.

Table 1
Thermal and physical properties of Ti and Mo [24,25,27].

Property	CpTi (grade 2)	Mo
Density, Kgm^{-3}	4500	10,220
Melting point, °C	1650–1670	2617
Boiling point, °C	3287	4640
Thermal conductivity, $Wm^{-1}K^{-1}$	17	138
Thermal diffusivity, m^2s^{-1}	7.15×10^{-6}	54.3×10^{-6}

electron microscope (SEM) analysis based on the protocol suggested by Struers [18]. The microhardness test was conducted with FM-700 Digital Vickers Microhardness Tester at a constant load of 200 g for 15 s. The tensile specimens were prepared according to E8/E8M ASTM standard. The samples were rectangular with a 10 mm gauge length, 2 mm width and 1 mm thickness, which was described as a mini sample [19]. The samples were tested with the MTS Criterion Model 43 Electromechanical Universal Test System machine at room temperature at a strain rate of 0.5 mm/min. The surface roughness of the samples was measured using Surftest SJ-210 portable surface roughness tester from Mitutoyo Corporation.

3. Results and discussions

3.1. Microstructure

With the selected optimum process parameters 3D samples (Fig. 1) were manufactured for the study.

The constituted SEM micrographs (Fig. 2) demonstrates a Ti15Mo alloy matrix of partially melted randomly distributed Mo parities embedded in the Ti alloy, observed from both the top (perpendicular) and side (longitudinal) directions of the 3D samples. The distribution and the mixing of the partially melted Mo particles in the solidified melt pool could be related to the convective flow in the liquid melt pool [20]. The convective melt flow pattern of the solidified melt pool is due to the inherent non-uniform distribution of the Gaussian laser beam that melts the metallic powders leading to a non-uniform temperature gradient of the molten pool [21]. The hydrodynamic movement of the molten liquid is governed by the temperature gradient in the molten pool. The temperature gradient induces recirculating flow within the molten pool which resulted in the dispersed and random distribution of the partially melted Mo particles in the Ti alloy matrix. Körner et al. [22] and Körner et al. [23], also pointed out that the Gaussian laser beam melting process is very complex, and it is governed by laser beam absorption, Marangoni flow, viscosity, surface tension, capillary effects, gravity, etc., which leads to stochastic melt flow of the molten liquid and the resultant random distribution of the partially melted Mo particles in the solidified alloy.

The partial melting of Mo is due to the thermophysical differences (Table 1) between the two elemental powders. Mo has a melting point of 2623 °C [24] while Ti has a melting point in the range of 1650–1670 °C [25], obviously with a temperature difference of almost 1000 °C Ti would melt completely before Mo. The laser reflectance of Mo is also higher than that of Ti [26], hence Mo powder particles would reflect more of the laser radiation while Ti would absorb more laser radiation than Mo. The higher absorptivity of the laser radiation by Ti cum the low melting point would cause it to melt first before Mo. The density of Mo is higher than that of Ti, which means it could sink to the bottom of the molten pool during the LPBF melting process and be shielded from the full intensity of the radiation of the laser beam. As a result, Mo could only be melted partially by the laser beam before the solidification process was completed.

The high rate of heating and cooling (10^4–10^6 K/s) [28,29] simultaneously of the LPBF process could also contribute to the partial melting of the Mo particles. The LPBF melting and solidification occurs very fast that the Mo particles could not melt completely before the solidification process. The thermal conductivity and thermal diffusivity (Table 1) of Mo is higher than Ti, which implies the rate of heat conduction between its particles should be higher than that of Ti. Hence, if the rate of the solidification could be controlled to occurs slowly, perhaps the Mo powder particles could have melted completely and form a homogenous microstructure before the solidification process. Vrancken et al. [30] also investigated the possibility of using the LPBF process to manufacture Ti6Al4V–10Mo through the in-situ alloying process. Ti6Al4V-ELI was mixed with 10 wt% Mo powder. The Ti6Al4V–10Mo microstructure presents partially melted Mo particles distributed randomly in the β-titanium alloy matrix, which concurs with the experiment. The gray and dark varying contract areas (Fig. 2) represent dissolved Mo in the Ti alloy matrix whiles the white contrasting areas represent the partially melted Mo particles.

The optical micrographs obtained for the Ti15Mo microstructure (Fig. 3) present three distinct phases; the partially melted Mo particles, gray and dark varying contrast areas as observed along the perpendicular and the longitudinal directions. The Ti15Mo micrographs are α+β microstructure with randomly dispersed partially melted Mo particles. Needles fine acicular martensite could be observed in the dark filed (Fig. 4A) and the SEM micrographs (Fig. 4B). The fine acicular martensites were woven inside the prior β grains. The martensitic nature of the micrographs corresponds to the general nature of LPBF micrographs due to the rapid solidification of the LPBF process. It is this rapid solidification process which reduces the ductility of the LPBF manufactured

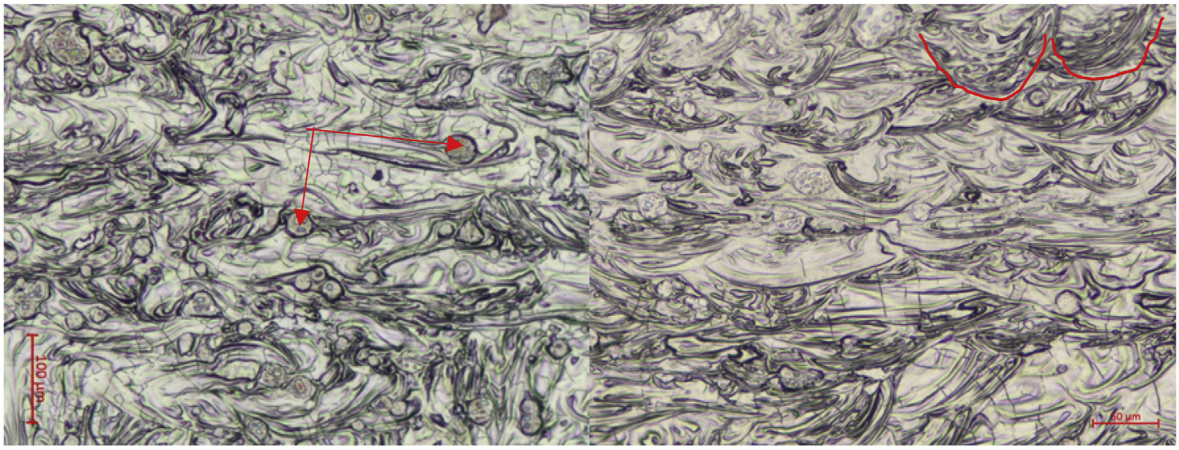

Fig. 3. Ti15Mo microstructure (A) Perpendicular view (B) Longitudinal view.

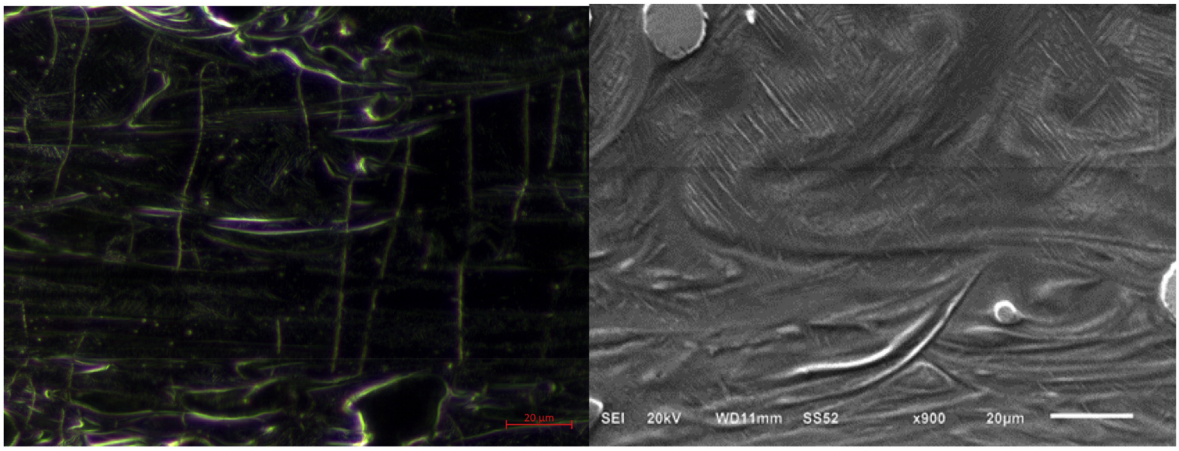

Fig. 4. Dark filed optical micrograph (A) SEM micrograph (B).

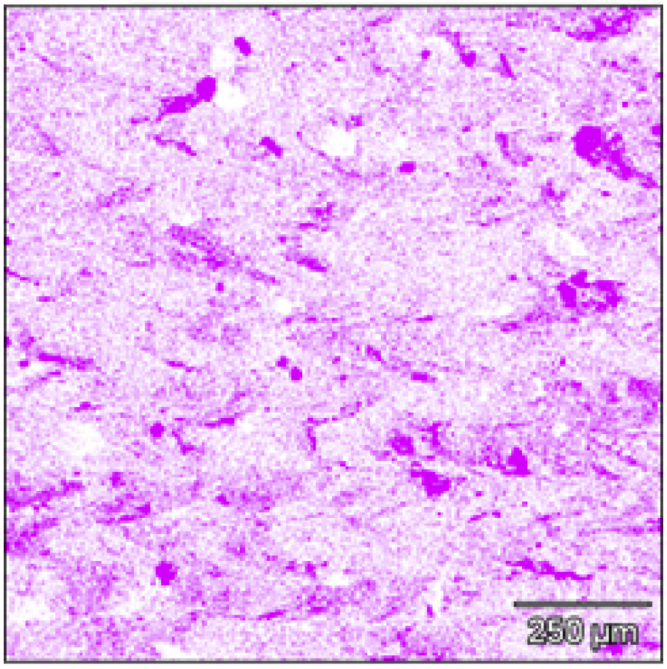

Fig. 5. EDS elemental mapping of Ti15Mo.

samples and induces other undesirable issues such as residual stress [31]. The wavy like nature of the micrograph (Fig. 4B) is due to the Marangoni flow (convective flow within the molten pool) [20].

EDS elemental mapping (Fig. 5) analysis was conducted to determine the distribution of Mo in the Ti matrix. Generally, the Mo distribution was the same in the perpendicular and longitudinal direction. Mo was evenly distributed in the Ti matrix with pockets of high concentration of Mo. The pockets of high contraction of Mo could be attributed to the hydrodynamics movement (convective flow) of the molten flow and the homogeneity of the Ti15Mo powder mixture before the in-situ alloying. When a pre-alloyed powder is used for manufacturing, each powder particle has the composition of the desired alloy composition in the final part [34] therefore producing a component with a homogeneous distribution of the alloying element. In the case of elemental powder mixture such as Ti15Mo used for the current experiment, the individual powder particle has an elemental composition of the element, therefore the individual elements could be distributed inhomogeneously in the alloy. The degree of the homogeneity of the Ti15Mo powder mixture could also

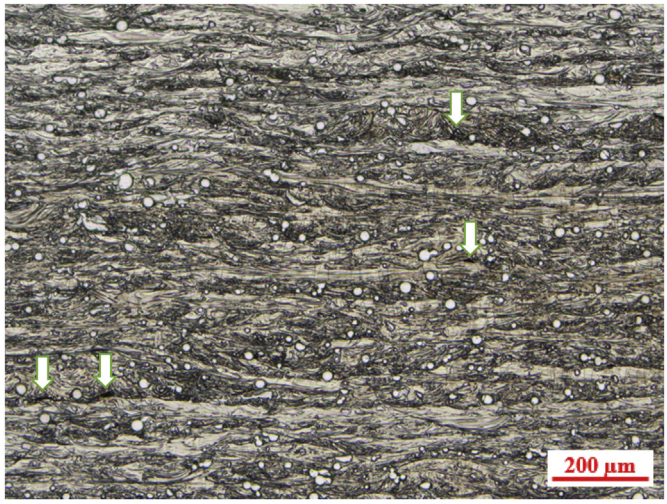

Fig. 6. Interlayer micropores in the Ti15Mo microstructure (white arrows).

contribute to the formation of the concentrated Mo pockets in the Ti15Mo alloy. Though every step was taken to mechanically mixed the Ti and Mo powder thoroughly to obtained homogenous mixture before the in-situ alloying. This observation of pockets of high concentration of Mo is similar to what was reported by Vrancken et al. [30] in their attempt to in situ alloy Ti6Al4V-ELI with 10 wt% Mo powder using LPBF manufacturing method.

Due to the single-track side-by-side and subsequent layer-by-layer manufacturing method of the LPBF process, the microstructure of Ti15Mo samples was examined for the presence of micropores. As already stated, the non-uniform distribution of the Gaussian laser beam during the LPBF melting process induces temperature difference in the molten pool which triggers surface tension gradient between the center and the edges of the molten metal [21]. The temperature gradient generates waves (Fig. 4B) in the liquid. The waves within the molten pool would amplify deformation and oscillation of the pool surface, and ripple formation as the molten metal solidifies leading to corrugated (rough) surfaces. The surface morphology of the solidified layer affects the even deposition of the powder on the previous layer. A rough surface would lead to inhomogeneous powder deposition, which would trigger inconsistency in the melt flow in the subsequent layers leading to interlayer pore formation.

Interlayer micropores were present (Fig. 6 – white arrow) in the Ti15Mo samples due to the morphology of the surface. A surface

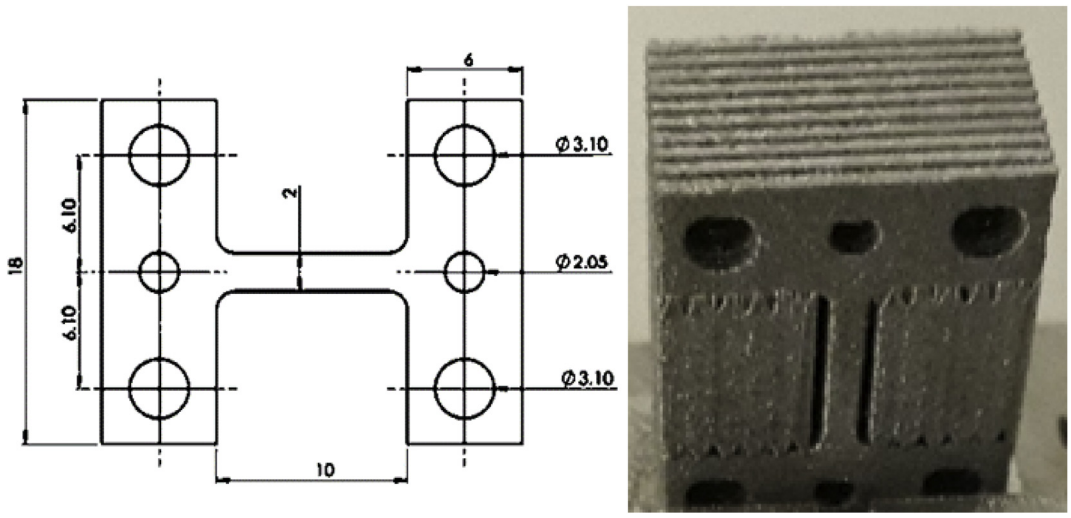

Fig. 7. Dimensions sketch of the tensile test samples (A) LPBF Ti15Momanufactured tensile test samples (B).

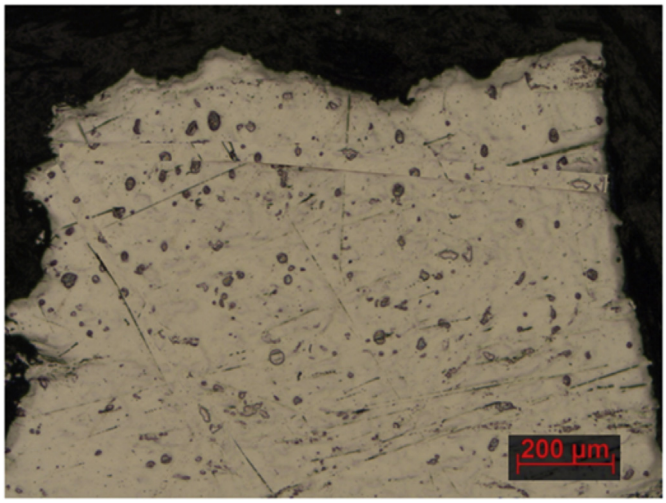

Fig. 8. Optical image of tensile test specimen showing the absence of gross necking before fracture.

roughness value of 35 µm for Rz was recorded in the perpendicular direction and 43 µm in the longitudinal direction of the samples. The high value of the surface roughness along the longitudinal direction (side) is due to the stair-step effect [32,33]. Due to the LPBF building mechanisms, measuring surface roughness from the perpendicular direction takes into account only one layer which is the last layer at the top. However, surface roughness along the side takes into consideration the multiple layers. The multiple interlayer connections and possible entrained powder particles that adhere and agglomerate to the external edge cumulatively increase the surface roughness value along the build direction (side). A similar observation was reported by Król & Tański [32]. The sizes of micropores due to the surface roughness were measured and were found less than 20 µm, hence the samples were considered as well-built dense 3D objects as reported elsewhere [31]. It was empirically proven and generally accepted that LPBF samples with pores size less than 20 µm would demonstrate stable mechanical properties for engineering applications and are therefore considered as dense well-built 3D objects [34].

3.2. *Mechanical properties*

Five of the prepared tensile test samples according to the E8/E8M

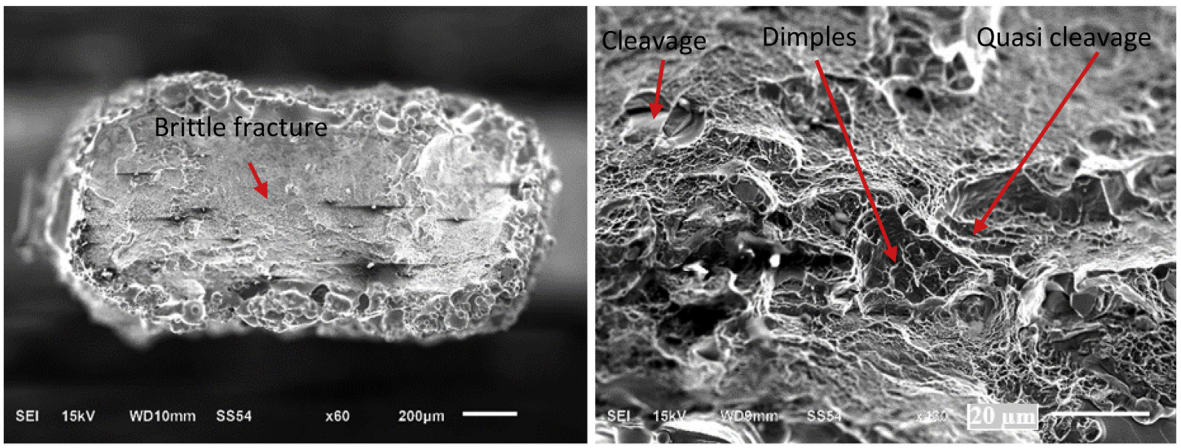

Fig. 9. SEM micrograph of fracture surface – total view (A) Fracture surface at higher magnification showing predominant brittle fracture with some cleavage features at fracture surface (B).

ASTM standard (Fig. 7) were tested. The samples were fixed with zero displacements in the x and z direction and were only allowed to move in the vertical direction (along the y-axis). The samples were pulled vertically and the motion in the vertical y-direction with the respect to the bottom plane was registered until the samples fractured (Fig. 8). The stress was determined as the ratio between the applied load and the nominal cross-section of the samples while the strain is taking as the ratio between the normal height and the increased height after the tensile test.

The fractured surface was rough and irregular without gross necking (Fig. 8) as expected of martensitic material. Ultimate tensile strength (UTS) value of 894 ± 24 MPa was recorded and the percentage of elongation was 2.8 ± 1.7%. This value compares to 858 ± 16 MPa reported by Vrancken et al. [30] for Ti6Al4V-ELI with 10 wt% Mo in situ alloyed using the LPBF manufacturing technology. The UTS obtained for the Ti15Mo alloy manufactured by the conventional methods ranges from 800 to 900 MPa [35] which is comparable to the LPBF UTS value. The percentage of elongation of Ti15Mo was reported as 16% by Disegi et al. [36] when manufactured by the conventional methods and heat treated.

Though the LPBF manufacturing process is considered as a renaissance of the manufacturing industry due to its freedom of design, the fast rate of heating and cooling leads to the martensitic formation which inevitably reduces the ductility of the Ti15Mo samples manufactured by the LPBF process.

SEM analysis of the fracture surface reveals the occurrence of complex ductile/brittle fracture (Fig. 9) with the predominance of brittle fracture (Fig. 9A), which explained the absence of gross necking before fracture (Fig. 8). There was evidence of areas of ductile tearing (quasi-cleavage fracture) (Fig. 9B). This type of fracture is due to the occurrence of both ductile (dimples) and brittle fracture together on a single fracture surface (mixed mode).

The microhardness of the samples was determined from the perpendicular and the longitudinal directions to study the anisotropic behaviour typical of LPBF build parts [35]. Due to the layerwise (step-by-step) building process used by the LPBF technology the microstructure and mechanical properties of LPBF build parts could be different when viewed from different directions [31,33,37]. The directional variation in the microstructure and the mechanical properties of LPBF built parts is due to the directional heat flux and the large thermal gradient [36,38]. The FM-700 Digital Vickers Microhardness Tester at a constant load of 200 g for 15 s was used to make 15 indentations on the surface of the Ti15Mo samples and the average calculated. A microhardness value of 410 ± 17 HV was recorded for the perpendicular direction and 441 ± 12 HV for the longitudinal direction. The difference in the microhardness values attest to the fact that LPBF build parts are not homogenous throughout the bulk material as reported in the literature. The microhardness values of the current experiment correlate with the result of Collins et al. [39]. They produced a compositionally graded structure of Ti-xMo (x = 0-25 at.%) by laser engineered net-shaping (LENS™) and reported a microhardness value of 450 HV at 10 wt% Mo concentration and noted that the microhardness value of the samples reduces with increasing Mo content.

As demonstrated by the current experiment and other previous research output [12,13], in-situ alloying is an efficient way to manufacture new materials, nevertheless, to manufacture homogeneous alloy is still a challenge that needs to be resolved. Perhaps for the current experiment using Mo powder of smaller particles size <45 μm or nano-powder particles could have resulted in the complete melting of the powder and improve the homogeneity of the alloy without pockets of concentrated Mo areas.

4. Conclusion

The study demonstrated that the LPBF process could be used to in-situ alloy different elemental powders successfully. The UTS and microhardness values obtained for the LPBF Ti15Mo were in the range of samples produced by the conventional methods, which shows that the LPBF methods of manufacturing could be used to produced 3D samples with mechanical properties comparable to the conventional methods. However, for the current experiment the inability of the laser beam to melt the Mo powder particles completely due to the thermophysical differences between the two materials, suggest that the idea of using the LPBF process for in-situ alloying different elemental powders for specific engineering and biomedical applications is still at its infant stage and further research is required to achieve complete melting and "absolute" homogeneity.

Credit author statement

The author was responsible for experimental work and writing of the manuscript.

Declaration of competing interest

The authors declare that they have no known competing financial interests or personal relationships that could have appeared to influence the work reported in this paper.

Acknowledgment

This work is based on the research supported by the South African Research Chairs Initiative of the Department of Science and Technology and National Research Foundation of South Africa (Grant Nº97994) and the Collaborative Program in Additive Manufacturing (Contract NºCSIR-NLC-CPAM-18-MOA-CUT-01). The author would like to acknowledge the contribution of Prof. I. Yadroitsau, Prof. P. Krakhmalev and Dr. I. Yadroitsava who were his doctoral studies supervisors.

References

[1] M. Júnior, J.R. Severino, R.A. Nogueira, R.O.D. Araújo, T.A.G. Donato, V.E. Arana-Chavez, A.P.R.A. Claro, J.C.S. Moraes, M.A.R. Buzalaf, C.R. Grandini, Preparation and characterization of Ti-15Mo alloy used as biomaterial, Mater. Res. 14 (1) (2011) 107–112.

[2] M. Niinomi, Mechanical properties of biomedical titanium alloys, Mater. Sci. Eng., A 243 (1) (1998) 231–236.

[3] V.R. Jablokov, M.J. Nutt, M.E. Richelsoph, H.L. Freese, The application of Ti-15Mo beta titanium alloy in high strength structural orthopaedic applications, in: Titanium, Niobium, Zirconium, and Tantalum for Medical and Surgical Applications, Journal of ASTM International vol. 2, 2006, 8.

[4] I. Yadroitsev, I. Shishkovsky, P. Bertrand, I. Smurov, Manufacturing of fine-structured 3D porous filter elements by selective laser melting, Appl. Surf. Sci. 255 (10) (2009) 5523–5527.

[5] L.E. Murr, S.M. Gaytan, F. Medina, H. Lopez, E. Martinez, B.I. Machado, D.H. Hernandez, L. Martinez, M.I. Lopez, R.B. Wicker, J. Bracke, Next-generation biomedical implants using additive manufacturing of complex, cellular and functional mesh arrays, Phil. Trans. Roy. Soc. Lond.: Mathematical, Physical and Engineering Sciences 368 (1917) 1999–2032, 2010.

[6] B.R.E.N.T. Stucker, Additive manufacturing technologies: technology introduction and business implications, in: Frontiers of Engineering: Reports on Leading-Edge Engineering from the 2011 Symposium, National Academies Press, Washington, DC, 2012, pp. 19–21.

[7] D. Buchbinder, H.B. Schleifenbaum, S. Heidrich, W. Meiners, J. Bültmann, High power selective laser melting (HP SLM) of aluminum parts, Physics Procedia 12 (2011) 271–278.

[8] J.J. Dunkley, Metal powder atomisation methods for modern manufacturing, Johnson Matthey's international journal of research exploring science and technology in industrial applications (2019) 226.

[9] H. Moheb-Alizadeh, R. Handfield, The impact of raw materials price volatility on cost of goods sold (COGS) for product manufacturing, IEEE Trans. Eng. Manag. 65 (2018) 460–473.

[10] W.J. Sames, F.A. List, S. Pannala, R.R. Dehoff, S.S. Babu, The metallurgy and processing science of metal additive manufacturing, Int. Mater. Rev. 6 (15) (2016) 315–360.

[11] S. Dadbakhsh, R. Mertens, L. Hao, J. Van Humbeeck, J.P. Kruth, "Selective laser melting to manufacture "in situ" metal matrix composites: a review", Adv. Eng. Mater. 21 (3) (2019) 1801244.

[12] A. Zenani, T.C. Dzogbewu, W.B. Du Preez, I. Yadroitsev, Optimum process parameters for direct metal laser sintering of Ti6Al powder blend, Universal journal of mechanical engineering 8 (4) (2020) 170–182.

[13] A. Kinnear, T.C. Dzogbewu, I. Yadroitsev, P. Krakhmalev, I. Yadroitsava, Manufacturing, microstructure and mechanical properties of selective laser melted Ti6Al4V-Cu, in: LiM" Lasers in Manufacturing" Conference, 2017. Munich.
[14] N.T. Aboulkhair, N.M. Everitt, I. Ashcroft, C. Tuck, Reducing porosity in AlSi10Mg parts processed by selective laser melting, Additive Manufacturing 1 (2014) 77–86.
[15] P. Vora, R. Martinez, N. Hopkinson, I. Todd, K. Mumtaz, Customised alloy blends for in-situ Al339 alloy formation using a nchorless Selective Laser Melting, Technologies 5 (2) (2017) 24.
[16] T.C. Dzogbewu, I. Yadroitsev, P. Krakhmalev, I. Yadroitsava, A. Du Plessis, Optimal process parameters for in-situ alloyed Ti15Mo structures by direct metal laser sintering, in: The 28th Annual International Solid Freeform Fabrication Symposium, University of Texas. Austin, 2017.
[17] I. Yadroitsev, P. Krakhmalev, I. Yadroitsava, Hierarchical design principles of selective laser melting for high quality metallic objects, Additive Manufacturing 7 (2015) 45–56.
[18] L. Bjerregaard, B. Geels, M. Ottesen, M. Ruckert, Metalog Guide, Struers A/S, 1996.
[19] I. van Zyl, M. Moletsane, P. Krakhmalev, I. Yadroitsava, I. Yadroitsev, Validation of miniaturised tensile testing on DMLS TI6AL4V (ELI) specimens, S. Afr. J. Ind. Eng. 27 (3) (2016) 192–200.
[20] S. Kou, C. Limmaneevichitr, P.S. Wei, Oscillatory Marangoni flow: a fundamental study by conduction-mode laser spot welding, Weld. J. 90 (12) (2011) 229–240.
[21] C.L. Chan, J. Mazumder, M.M. Chen, Three-dimensional axisymmetric model for convection in laser-melted pools, Mater. Sci. Technol. 3 (4) (1987) 306–311.
[22] C. Körner, E. Attar, P. Heinl, Mesoscopic simulation of selective beam melting processes, J. Mater. Process. Technol. 211 (6) (2011) 978–998.
[23] C. Körner, A. Bauereiß, E. Attar, Fundamental consolidation mechanisms during selective beam melting of powder, Model. Simulat. Mater. Sci. Eng. 21 (8) (2013), 085011.
[24] AZO, AZO Materials, 2015 [Online]. Available: http://www.azom.com. (Accessed 7 April 2020).
[25] ASM, ASM aerospace specification metals Inc [Online]. Available: http://www.matweb.com, 2016. (Accessed 7 April 2020).
[26] D. Lynch, W. Hunter, E. Palik, Handbook of Optical Constants of Solids, Academic press, Orlando, 1985.
[27] Glemco, Molybdenum, Mo (wt 100%) material notes [Online]. Available: www.glemco.com, 2016. (Accessed 5 April 2020).
[28] I.A. Roberts, C.J. Wang, R. Esterlein, M. Stanford, D.J. Mynors, A three-dimensional finite element analysis of the temperature field during laser melting of metal powders in additive layer manufacturing, Int. J. Mach. Tool Manufact. 49 (12) (2009) 916–923.
[29] E. Brandl, D. Greitemeier, Microstructure of additive layer manufactured Ti–6Al–4V after exceptional post heat treatments, Mater. Lett. 81 (2012) 84–87.
[30] B. Vrancken, L. Thijs, J. Kruth, J. Van Humbeeck, Microstructure and mechanical properties of a novel β titanium metallic composite by selective laser melting, Acta Mater. 68 (2014) 150–158.
[31] T. Becker, M. Van Rooyen, D. Dimitrov, Heat treatment of Ti-6Al-4V produced by lasercusing, S. Afr. J. Ind. Eng. 26 (2) (2015) 93–103.
[32] M. Król, T. Tański, Surface quality research for selective laser melting of Ti-6Al-4V alloy, Arch. Metall. Mater. 61 (3) (2016) 1291–1296.
[33] K. Kempen, E. Yasa, L. Thijs, J.P. Kruth, J. Van Humbeeck, Microstructure and mechanical properties of selective laser melted 18Ni-300 steel, Physics Procedia 12 (2011) 255–263.
[34] T.C. Dzogbewu, L. Monaheng, J. Els, I. van Zyl, W.B. du Preez, I. Yadroitsava, I. Yadroitsev, Evaluation of the compressive mechanical properties of cellular DMLS structures for biomedical applications, in: 17th RAPDASA Annual International Conference, Vanderbijlpark, South Africa, 2016.
[35] ATI, Ti-15Mo beta titanium alloy. Technical data sheet, in: Allegheny Technologies Incorporated 1000 Six PPG Place Pittsburgh, 2014, pp. 15222–15479. USA, www.ATImetals.com.
[36] J.A. Disegi, M.D. Roach, R.D. McMillan, B.T. Shultzabarger, Alpha plus beta annealed and aged Ti-15 Mo alloy for high strength implant applications, J. Biomed. Mater. Res. B Appl. Biomater. 105 (7) (2017) 2010–2018.
[37] L. Thijs, F. Verhaeghe, T. Craeghs, J. Van Humbeeck, J.P. Kruth, A study of the microstructural evolution during selective laser melting of Ti–6Al–4V, Acta Mater. 58 (9) (2010) 3303–3312.
[38] J.P. Kruth, M. Badrossamay, E. Yasa, J. Deckers, L. Thijs, J. Van Humbeeck, Part and material properties in selective laser melting of metals, in: Proceedings of the 16th International Symposium on Electromachining, 2010, pp. 1–12.
[39] P. Collins, R. Banerjee, S. Banerjee, H. Fraser, Laser deposition of compositionally graded titanium–vanadium and titanium–molybdenum alloys, Mater. Sci. Eng., A 352 (1) (2003) 118–128.